8200 *Inorg. Chem.* **2010**, *49*, 8200–8207
DOI: 10.1021/ic100806w

Inorganic Chemistry
Article

Electronic Structural Comparison of the Reactions of Dioxygen and Alkenes with Nitrogen-Chelated Palladium(0)

Brian V. Popp, Christine M. Morales,† Clark R. Landis,* and Shannon S. Stahl*

Department of Chemistry, University of Wisconsin-Madison, 1101 University Avenue, Madison, Wisconsin 53706. †Current address: Department of Chemistry, University of Wisconsin-Eau Claire, Phillips 430, Eau Claire, WI 54702-4004

Received April 24, 2010

The reaction of molecular oxygen with palladium(0) centers is a key step in Pd-catalyzed aerobic oxidation reactions. The present study provides a density functional theory (DFT) computational analysis of the mechanism and electronic structural features of the reversible, associative exchange between O_2 and ethylene at an ethylenediamine (en)-coordinated palladium(0) center. Salient features of the mechanism include: (1) the near thermoneutrality of the O_2-alkene exchange reaction, consistent with experimentally observed reversible exchange between O_2 and alkenes at well-defined Pd centers, (2) end-on activation of triplet O_2 at an apical site of the trigonal Pd^0 center, resulting in formation of a $Pd^I(\eta^1$-superoxide) species, (3) rearrangement of the $Pd^I(\eta^1$-superoxide) species into a pseudo-octahedral (en)$Pd(\eta^2$-$O_2)(\eta^2$-$C_2H_4)$ species with concomitant crossing from the triplet to singlet energy surfaces, and (4) release of alkene from an axial face of (en)$Pd^{II}(\eta^2$-peroxo) with a geometry in which the alkene leaves with an end-on trajectory (involving an interaction of the Pd d_{z^2} and alkene π^* orbitals). This study highlights the similar reactivity and reaction pathways of alkenes and O_2 with an electron-rich metal center, despite the different ground-state electronic configurations of these molecules (closed-shell singlet and open-shell triplet, respectively).

Introduction

Palladium(II)-catalyzed oxidation reactions have a rich history in the field of transition-metal chemistry and catalysis, and they continue to emerge as valuable methods for the selective oxidation of organic molecules.[1] In many cases, these reactions proceed by a two-stage oxidase-style mechanism depicted schematically in Scheme 1. According to this mechanism, Pd^{II} mediates the two-electron oxidation of an organic substrate, resulting in the formation of Pd^0 and 2 equiv of H^+. The Pd^{II} catalyst is regenerated by oxidation of Pd^0 with an oxidant. Copper(II) salts and *p*-benzoquinone are among the most widely used oxidants, but increasing attention has focused on methods capable of using O_2 as the sole stoichiometric oxidant.[2] Despite recent advances in the development of direct dioxygen-coupled Pd-catalyzed oxidation reactions, limitations remain, and many reactions still require the use of oxidants other than O_2. In this context, the mechanism of direct oxidation of reduced Pd species by molecular oxygen has been the subject of considerable study by us and others.[3,4] The reaction of O_2 with catalytically relevant Pd^0 model complexes has been a major area of emphasis.[5]

Bathocuproine (bc = 2,9-dimethyl-4,7-diphenyl-1,10-phenanthroline) is a chelating nitrogen ligand that has been employed in oxidase-type Pd-catalyzed methods for producing H_2O_2 from molecular oxygen in the presence of sacrificial reductants (Scheme 1: $SubH_2$ = CO/H_2O or RCH_2OH).[6] These results provided the inspiration for our previous studies, in which we investigated the reactions of molecular oxygen with well-defined (bc)$Pd^0(\eta^2$-alkene) complexes, **1** and **2^X** (eqs 1 and 2),[3a,7] which yield the η^2-peroxo complex (bc)$Pd^{II}(\eta^2$-$O_2)$ (**3**) [alkene = dibenzylideneacetone, dba, or para-substituted β-nitrostyrene derivatives, ns^X].[3a,d]

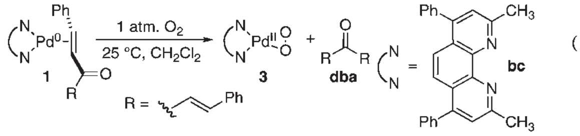

(1)

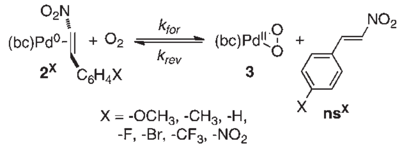

(2)

Kinetic studies of the reaction of O_2 with (bc)Pd^0(dba) (**1**) revealed the presence of a bimolecular rate law,

---

*To whom correspondence should be addressed. E-mail: stahl@chem.wisc.edu (S.S.S.), landis@chem.wisc.edu (C.R.L.).

(1) (a) Tsuji, J. *Palladium Reagents and Catalysts: New Perspectives for the 21st Century*; John Wiley & Sons: Hoboken, 2004. (b) Henry, P. M. *Palladium Catalyzed Oxidation of Hydrocarbons*; Kluwer: Boston, 1980.

Scheme 1. General Catalytic Cycle for Pd^{II}-Catalyzed Oxidation Reactions

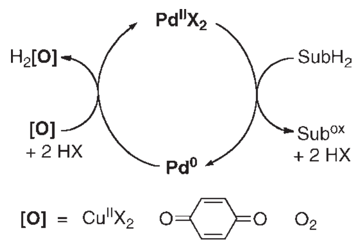

rate = $k[\mathbf{1}]\cdot[O_2]$, and a large negative entropy of activation, $\Delta S^{\ddagger} = -43$ e.u.[7a] These results contrasted the pathways that have been observed for oxidative addition of aryl halides to related L_2Pd^0-dba complexes, which exhibit dissociative or parallel associative/dissociative pathways.[8] A Hammett analysis of k_{for} for oxygenation of complexes $\mathbf{2^X}$ (eq 2) revealed that electron-donating substituents enhance the rate of the reaction, as expected for a reaction involving "oxidative addition" of O_2 to the Pd^0 center. Finally, the reactions of O_2 with $\mathbf{2^X}$ were shown to be approximately thermoneutral. Addition of excess ns^X to the peroxo-Pd^{II} species **3** resulted in displacement of O_2 from the Pd^{II} center and formation of the Pd^0-alkene complex (k_{rev}, eq 2).[9] The mechanistic observations for O_2-alkene exchange closely resemble independent results obtained from the study of alkene−alkene exchange at Pd^0-alkene complexes (eq 3).[7b] Collectively, the results draw attention to the distinct similarity between the reactivity of electron-deficient alkenes and molecular oxygen at closed-shell Pd centers, a similarity that belies the fundamental difference between the electronic structure of the two substrates: olefins have well-defined donor (filled π) and acceptor (empty π^*) orbitals, whereas dioxygen has two singly occupied π^* orbitals resulting in a triplet electronic ground-state.

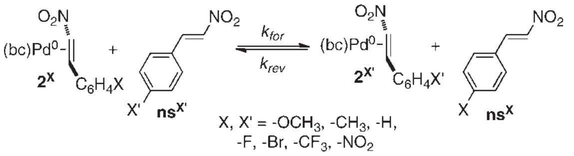

(3)

In our initial effort to elucidate the electronic structural principles underlying the reaction of triplet O_2 with closed-shell singlet Pd^0 centers, we employed density functional theory (DFT) computational methods to investigate the pathway for reaction of a simple (en)Pd^0 (en = ethylenediamine) fragment with O_2.[3b,10] The results of this initial study revealed that dioxygen reacts with Pd^0 by a stepwise process, summarized in eq 4: (1) initial formation of a triplet η^1-superoxo-Pd^I adduct, (2) spin-crossover from the triplet to the singlet surface, and (3) collapse of the singlet η^1-superoxo-Pd(I) adduct into an η^2-peroxo-Pd(II) complex.[11] Delocalization of spin density from triplet-O_2 onto the palladium center in the first step reduces the exchange interaction between the unpaired spins and facilitates crossover from the triplet to singlet surface. Spin-crossover at the minimum-energy crossing point (MECP) enables formation of the second Pd−O bond, which leads to the singlet η^2-peroxo-Pd^{II} complex. In the present study, we expand upon these preliminary results by investigating the reaction of O_2 with (en)Pd(η^2-C_2H_4), **4**, a complex that more closely resembles the Pd^0-alkene complexes that have been the focus of experimental investigations. The results outlined below provide valuable electronic structural insights into the similarities and differences between reactions of O_2 and alkenes with Pd^0.

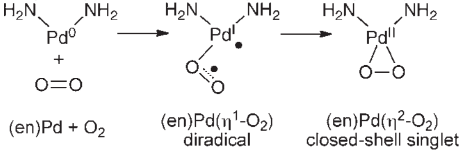

(4)

Computational Methods

All calculations were performed using spin-unrestricted density functional theory (UDFT)[12] as implemented in the

---

(2) (a) Stahl, S. S. *Science* **2005**, *309*, 1824–1826. (b) Stahl, S. S. *Angew. Chem., Int. Ed.* **2004**, *43*, 3400–3420. (c) Stoltz, B. M. *Chem. Lett.* **2004**, *33*, 362–367. (d) Sigman, M. S.; Schultz, M. J. *Org. Biomol. Chem.* **2004**, *2*, 2551–2554. (e) Sigman, M. S.; Jensen, D. R. *Acc. Chem. Res.* **2006**, *39*, 221–229. (f) Nishimura, T.; Uemura, S. *Synlett* **2004**, 201–216. (g) Sheldon, R. A.; Arends, I. W. C. E.; ten Brink, G.-J.; Dijksman, A. *Acc. Chem. Res.* **2002**, *35*, 774–781. (h) Toyota, M.; Ihara, M. *Synlett* **2002**, 1211–1222.

(3) The ligand-modulated reactivity of reduced Pd complexes with dioxygen has been reported with neutral, cis-chelating imine and amine ligands, see: (a) Stahl, S. S.; Thorman, J. L.; Nelson, R. C.; Kozee, M. A. *J. Am. Chem. Soc.* **2001**, *123*, 7188–7189. (b) Landis, C. R.; Morales, C. M.; Stahl, S. S. *J. Am. Chem. Soc.* **2004**, *126*, 16302–16303. (c) Keith, J. M.; Nielsen, R. J.; Oxgaard, J.; Goddard, W. A., III *J. Am. Chem. Soc.* **2005**, *127*, 13172–13179. (d) Popp, B. V.; Thorman, J. L.; Stahl, S. S. *J. Mol. Catal. A: Chem.* **2006**, *251*, 2–7. (e) Keith, J. M.; Goddard, W. A., III; Oxgaard, J. *J. Am. Chem. Soc.* **2007**, *129*, 10361–10369; N-heterocyclic carbene ligands, see:. (f) Konnick, M. M.; Guzei, I. A.; Stahl, S. S. *J. Am. Chem. Soc.* **2004**, *126*, 10212–10213. (g) Nielsen, R. J.; Goddard, W. A., III *J. Am. Chem. Soc.* **2006**, *128*, 9651–9660. (h) Konnick, M. M.; Gandhi, B. A.; Guzei, I. A.; Stahl, S. S. *Angew. Chem., Int. Ed.* **2006**, *45*, 2904–2907. (i) Yamashita, M.; Goto, K.; Kawashima, T. *J. Am. Chem. Soc.* **2005**, *127*, 7294–7295. (j) Popp, B. V.; Wendlandt, J. E.; Landis, C. R.; Stahl, S. S. *Angew. Chem., Int. Ed.* **2007**, *46*, 601–604. (k) Popp, B. V.; Stahl, S. S. *J. Am. Chem. Soc.* **2007**, *129*, 4410–4422. (l) Konnick, M. M.; Stahl, S. S. *J. Am. Chem. Soc.* **2008**, *130*, 5753–5762. (m) Chowdhury, S.; Rivalta, I.; Russo, N.; Sicilia, E. *Chem. Phys. Lett.* **2008**, *456*, 41–46. (n) Chowdhury, S.; Rivalta, I.; Russo, N.; Sicilia, E. *J. Chem. Theory Comput.* **2008**, *4*, 1283–1292; Neutral, monodentate imine and amine ligands, see:. (o) Popp, B. V.; Stahl, S. S. *Chem.—Eur. J.* **2009**, *15*, 2915–2922. (p) Keith, J. M.; Goddard, W. A., III *J. Am. Chem. Soc.* **2009**, *131*, 1416–1425; Metalated, bidentate aryl-imine ligands, see:. (q) Privalov, T.; Linde, C.; Zetterberg, K.; Moberg, C. *Organometallics* **2005**, *24*, 885–893; Dimethylsulfoxide ligands, see:. (r) Zierkiewicz, W.; Privalov, T. *Organometallics* **2005**, *24*, 6019–6028; Pincer-type, tridentate ligands, see:. (s) Denney, M. C.; Smythe, N. A.; Cetto, K. L.; Kemp, R. A.; Goldberg, K. I. *J. Am. Chem. Soc.* **2006**, *128*, 2508–2509. (t) Keith, J. M.; Muller, R. P.; Kemp, R. A.; Goldberg, K. I.; Goddard, W. A., III; Oxgaard, J. *Inorg. Chem.* **2006**, *45*, 9631–9633. (u) Chowdhury, S.; Rivalta, I.; Russo, N.; Sicilia, E. *Chem. Phys. Lett.* **2007**, *443*, 183–189; Phosphine ligands, see:. (v) Lanci, M. P.; Brinkley, D. W.; Stone, K. L.; Smirnov, V. V.; Roth, J. P. *Angew. Chem., Int. Ed.* **2005**, *44*, 7273–7276. (w) Smirnov, V. V.; Brinkley, D. W.; Lanci, M. P.; Karlin, K. D.; Roth, J. P. *J. Mol. Catal. A: Chem.* **2006**, *251*, 100–107; Hydroxide ligand in the gas phase, see:. (x) Schlangen, M.; Schwarz, H. *Helv. Chim. Acta* **2008**, *91*, 379–386. (y) Zhang, X.; Schlangen, M.; Baik, M.-H.; Dede, Y.; Schwarz, H. *Helv. Chim. Acta* **2009**, *92*, 151–164.

(4) The fundamental reactivity of dioxygen with mid-to-late-transition-metal complexes and metalloenzymes has been of interest for many decades; for reviews and a recent monograph, see: (a) Valentine, J. S. *Chem. Rev.* **1973**, *73*, 235–245. (b) Bytheway, I.; Hall, M. B. *Chem. Rev.* **1994**, *94*, 639–658. (c) *Activation of Small Molecules: Organometallic and Bioinorganic Perspectives*; Tolman, W. B., Ed.; Wiley-VCH: Weinheim, Germany, 2006; pp 159−234 and references therein.

(5) For overviews of the issues relevant to aerobic reoxidation during catalysis, see: (a) Popp, B. V.; Stahl, S. S. *Top. Organomet. Chem.* **2007**, *22*, 149–189. (b) Gligorich, K. M.; Sigman, M. S. *Angew. Chem., Int. Ed.* **2006**, *45*, 6612–6615. (c) Muzart, J. *Chem.—Asian J.* **2006**, *1*, 508–515.

(6) (a) Bianchi, D.; Bortolo, R.; D'Aloisio, R.; Ricci, M. *Angew. Chem., Int. Ed.* **1999**, *38*, 706–708. (b) Bianchi, D.; Bortolo, R.; D'Aloisio, R.; Ricci, M. *J. Mol. Catal. A: Chem.* **1999**, *150*, 87–94. (c) Bortolo, R.; Bianchi, D.; D'Aloisio, R.; Querci, C.; Ricci, M. *J. Mol. Catal. A: Chem.* **2000**, *153*, 25–29. (d) Querci, C.; D'Aloisio, R.; Bortolo, R.; Ricci, M.; Bianchi, D. *J. Mol. Catal. A: Chem.* **2001**, *176*, 95–100.

Gaussian 98 and Gaussian 03 electronic structure packages.[13] Our computational model system employed the ethylenediamine ligand (en) on the basis of geometric and energetic comparison with other diamine and diimine-based ligand systems (Supporting Information, Figure S1 and Table S1). The hybrid exchange functional, B3LYP,[14] was identified as the optimal functional based on the energetics of oxygenation as well as the optimized geometry of triplet O_2 (Supporting Information, Table S2).[15] The basis set used for all calculations was composed of the Stuttgart RSC 1997 ECP[16] for Pd, and the all-electron 6-311++G(d,p)[17] basis for all other atoms. Natural Bond Orbital (NBO) methods, as implemented in NBO 5.0 and 5.9,[18,19] were used to determine natural charges, spin densities, and Wiberg bond indices from converged spin-unrestricted density matrices.[20]

Full geometry optimizations were carried out in internal coordinates using the default Berny algorithm within Gaussian 03.[21] Relaxed total energy surface scans, in which all coordinates were optimized with the exception of the scanned metrical parameter, were carried out with Gaussian 98. Transition states were optimized using standard methods, and were followed by IRC calculations to verify that the transition state corresponds to the appropriate reactant/product potential energy surface.[22] Normal-mode analyses were performed at fully optimized geometries and transition states, confirming that each optimized minimum has zero imaginary frequencies and each optimized transition state has exactly one imaginary frequency. All geometry optimization and normal-mode calculations were performed with a polarizable continuum model (PCM) to mimic the solvation effect of the reaction medium. Zero-point energy, thermal corrections, and entropic corrections were estimated from the calculated frequencies.

Dipole-PCM (DPCM),[23,24] default in Gaussian 98, was used to initiate these studies; the integral-equation-formalism PCM (IEF-PCM),[25] default in Gaussian 03, was used to complete the studies. All geometries and energies reported, except where otherwise noted, are based on the latter solvation model. These calculations were used to predict the solvation free energy under experimental reaction conditions (i.e., CH_2Cl_2 solvent at 25 °C (298 K)). The solvation cavity was generated using UA0 radii with a scaling factor of 1.2. The physical characteristics of CH_2Cl_2 were defined using a dielectric constant of 8.93 and solvent probe radius of 2.27 Å.

We report both solvation-corrected total energies (ΔE_{sol}) (eq 5) and Gibbs' free energies at 298 K ($\Delta G_{298\mathrm{K}}$) (eqs 5−8). The entropy (S) is determined using gas-phase (1 atm) standard-state conditions. This necessitates that an additional energy correction (S_{corr}), added to the translation entropy component of the gas-phase entropy, be applied to convert to solution (1 M) standard-state conditions (eq 8) where n = no.

$$E_{sol} = E_{tot} + G_{sol} \tag{5}$$

$$H_{298\mathrm{K}} = E_{sol} + \sum_i \frac{1}{2} h\nu_i + \sum_i \frac{h\nu_i}{e^{h\nu_i/k_{\mathrm{B}}T} - 1} + \frac{n}{2} k_{\mathrm{B}} T \tag{6}$$

of rotational and translational modes

$$G_{298\mathrm{K}} = H_{298\mathrm{K}} + T \cdot S + T \cdot S_{corr} \tag{7}$$

$$S_{corr} = R \cdot \ln\left(\frac{R \cdot T}{P}\right) \tag{8}$$

The electronic configuration of converged SCF wave functions was confirmed by two methods: first, the value of $\langle S^2 \rangle$, which is ~1.0 for spin-contaminated open-shell singlet (OSS), 0.0 for closed-shell singlet (CSS), and ~2.0 for open-shell triplet (OST); and second, natural spin densities and Lewis structures. Spin-projection corrections were applied to the

---

(7) (a) Stahl, S. S.; Thorman, J. L.; de Silva, N.; Guzei, I. A.; Clark, R. W. *J. Am. Chem. Soc.* **2003**, *125*, 12–13. (b) Popp, B. V.; Thorman, J. L.; Morales, C. M.; Landis, C. R.; Stahl, S. S. *J. Am. Chem. Soc.* **2004**, *126*, 14832–14842.

(8) Amatore, C.; Jutand, A. *Coord. Chem. Rev.* **1998**, *178−180*, 511–528.

(9) Popp, B. V.; Stahl, S. S. *J. Am. Chem. Soc.* **2006**, *128*, 2804–2805.

(10) Theoretical methods have played a significant role in recent studies of dioxygen reactivity with late-transition-metal complexes and metalloenzymes; for examples, see: (a) Cramer, C. J.; Tolman, W. B. *Acc. Chem. Res.* **2007**, *40*, 601–608. (b) Roth, J. P. *Acc. Chem. Res.* **2009**, *42*, 399–408. (c) Aboelella, N. W.; Kryatov, S. V.; Gherman, B. F.; Brennessel, W. W.; Young, V. G., Jr.; Sarangi, R.; Rybak-Akimova, E. V.; Hodgson, K. O.; Hedman, B.; Solomon, E. I.; Cramer, C. J.; Tolman, W. B. *J. Am. Chem. Soc.* **2004**, *126*, 16896–16911. (d) Yu, H.; Fu, Y.; Guo, Q.; Lin, Z. *Organometallics* **2009**, *28*, 4443–4451. (e) Häller, L. J. L.; Mas-Marzá, E.; Moreno, A.; Lowe, J. P.; Macgregor, S. A.; Mahon, M. F.; Pregosin, P. S.; Whittlesey, M. K. *J. Am. Chem. Soc.* **2009**, *131*, 9618–9619. (f) Praetorius, J. M.; Allen, D. P.; Wang, R.; Webb, J. D.; Grein, F.; Kennepohl, P.; Crudden, C. M. *J. Am. Chem. Soc.* **2008**, *130*, 3724–3725. (g) Siegbahn, P. E. M.; Borowski, T. *Acc. Chem. Res.* **2006**, *39*, 729–738. (h) Gherman, B. F.; Baik, M.-H.; Lippard, S. J.; Friesner, R. A. *J. Am. Chem. Soc.* **2004**, *126*, 2978–2990.

(11) Similar sequential single-electron-transfer pathways have been proposed for side-on dioxygen binding at group 8, 9, and 11 closed-shell metal complexes; see references10c−10e.

(12) Koch, W.; Holthausen, M. C. *A Chemist's Guide to Density Functional Theory*; Wiley-VCH: Weinheim, Germany, 2000.

(13) (a) Frisch, M. J. et al. *Gaussian 98*, Revision A.9; Gaussian, Inc.: Pittsburgh, PA, 2001. (b) Frisch, M. J. et al. *Gaussian 03*, Revision D.01; Gaussian, Inc.: Wallingford, CT, 2004. See the Supporting Information for the full citations.

(14) (a) Becke, A. D. *J. Chem. Phys.* **1993**, *98*, 1372–1377. (b) Lee, C.; Yang, W.; Parr, R. G. *Phys. Rev. B* **1988**, *37*, 785–789.

(15) For a full discussion of the computational model system and method benchmarking see the Supporting Information.

(16) (a) The Stuttgart RSC 1997 ECP basis set for Pd was obtained from the Extensible Computational Chemistry Environment Basis Set Database, Version 02/25/04, as developed and distributed by the Molecular Science Computing Facility, Environmental and Molecular Sciences Laboratory which is part of the Pacific Northwest Laboratory, P.O. Box 999, Richland, Washington 99352, U.S.A., and funded by the U.S. Department of Energy. The Pacific Northwest Laboratory is a multi-program laboratory operated by Battelle Memorial Institute for the U.S. Department of Energy under contract DE-AC06-76RLO 1830. Contact Karen Schuchardt for further information. (b) Andrae, D.; Häussermann, U.; Dolg, M.; Stoll, H.; Preuss, H. *Theor. Chim. Acta* **1990**, *77*, 123–141.

(17) (a) Hehre, W. J.; Radom, L.; Schleyer, P. v. R.; Pople, J. A. *Ab Initio Molecular Orbital Theory*; Wiley: New York, 1986. (b) Krishnan, R.; Binkley, J. S.; Seeger, R.; Pople, J. A. *J. Chem. Phys.* **1980**, *72*, 650–654. (c) Mclean, A. D.; Chandler, G. S. *J. Chem. Phys.* **1980**, *72*, 5639–5648. (d) Clark, T.; Chandrasekhar, J.; Spitznagel, G. W.; Schleyer, P. v. R. *J. Comput. Chem.* **1983**, *4*, 294–301. (e) Frisch, M. J.; Pople, J. A.; Binkley, J. S. *J. Chem. Phys.* **1984**, *80*, 3265–3269.

(18) NBO 5.0, Glendening, E. D.; Badenhoop, J. K.; Reed, A. E.; Carpenter, J. E.; Bohmann, J. A.; Morales, C. M.; Weinhold, F. Theoretical Chemistry Institute, University of Wisconsin: Madison, WI, 2001.

(19) Reed, A. E.; Weinstock, R. B.; Weinhold, F. *J. Chem. Phys.* **1985**, *83*, 735–746.

(20) Natural charges and Wiberg bond indices parallel the extent of O−O and C−C bond reduction over the associative substitution pathway as judged by the respective bond length of the dioxygen and ethylene ligand. See Supporting Information, Table S3.

(21) Peng, C.; Ayala, P. Y.; Schlegel, H. B.; Frisch, M. J. *J. Comput. Chem.* **1996**, *17*, 49–56.

(22) (a) Gonzalez, C.; Schlegel, H. B. *J. Chem. Phys.* **1989**, *90*, 2154–2161. (b) Gonzalez, C.; Schlegel, H. B. *J. Phys. Chem.* **1990**, *94*, 5523–5527.

(23) For an overview of solvation models and reviews on PCM methods, see: (a) Cramer, C. J. *Essentials of Computational Chemistry: Theories and Models*; Wiley: Chichester, 2002. (b) Cramer, C. J.; Truhlar, D. G. *Chem. Rev.* **1999**, *99*, 2161–2200. (c) Tomasi, J.; Mennucci, B.; Cammi, R. *Chem. Rev.* **2005**, *105*, 2999–3093.

(24) (a) Miertuš, S.; Scrocco, E.; Tomasi, J. *Chem. Phys.* **1981**, *55*, 117–129. (b) Miertuš, S.; Tomasi, J. *Chem. Phys.* **1982**, *65*, 239–245. (c) Cossi, M.; Barone, V.; Cammi, R.; Tomasi, J. *Chem. Phys. Lett.* **1996**, *255*, 327–335.

(25) (a) Cancès, E.; Mennucci, B.; Tomasi, J. *J. Chem. Phys.* **1997**, *107*, 3032–3041. (b) Mennucci, B.; Tomasi, J. *J. Chem. Phys.* **1997**, *106*, 5151–5158. (c) Mennucci, B.; Cancès, E.; Tomasi, J. *J. Phys. Chem. B* **1997**, *101*, 10506–10517. (d) Tomasi, J.; Mennucci, B.; Cancès, E. *J. Mol. Struct.* (*Theochem*) **1999**, *464*, 211–226.

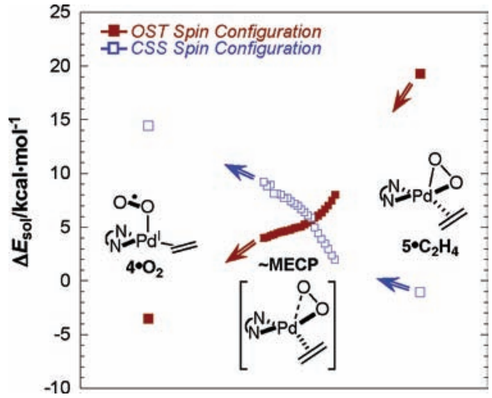

Figure 1. Location of an approximate MECP structure where intersystem spin-crossing is predicted.

spin-contaminated OSS total energy ($^1E_{\mathrm{UDFT}}$) to obtain the spin-corrected (SC) OSS total energy ($^1E_{\mathrm{SC}}$) following the method of Yamaguchi et al. to estimate the extent of triplet spin contamination in the OSS total energy (eqs 9 and 10).[26] This method yields a reasonable correction to the energy difference between the spin-contaminated wave function of the first excited state ($^1\Delta_g$) and triplet ground state ($^3\Sigma_g^-$) of dioxygen.[27]

$$^1E_{SC} = {}^1E_{UDFT} + f_{SC}[{}^1E_{UDFT} - {}^3E_{DFT}] \qquad (9)$$

where

$$f_{SC} \approx \frac{^1\langle S^2\rangle}{^3\langle S^2\rangle - {}^1\langle S^2\rangle} \qquad (10)$$

The MECP, between solvated singlet and triplet surfaces, was estimated by allowing the high-energy OST configuration of the CSS intermediate (e.g., $5 \cdot C_2H_4$) to relax to the ground-state OST configuration. At select geometries along the OST minimum energy path, SCF calculations specifying an unrestricted singlet configuration were carried out. The intersection of the resulting paths led to an approximate MECP geometry (Figure 1). These coordinates were then used as the starting point for the seam-search method of Harvey et al. with Gaussian 98.[28] This calculation included DPCM solvation during the optimization procedure. IEF-PCM single-point energy calculations were performed at the optimized MECP geometry. At the geometry-optimized MECP, the triplet-singlet energy gap is calculated to be less than 0.1 kcal/mol. Normal-mode analyses and the corresponding thermochemical corrections were not calculated explicitly at the MECP; nevertheless, an estimate was obtained using the thermal and entropic contributions calculated for the geometrically similar transition state $[\mathbf{4}\cdot\mathbf{O_2}]^{\mathbf{TS}}$.[29]

Results and Discussion

Structure of Pd(η^2-alkene) and Pd(η^2-peroxo) Model Complexes. We initiated our studies by optimizing the ground-state structure of (en)Pd(η^2-C_2H_4), **4**. The Pd^0-ethylene complex **4** resembles the complexes (bc)Pd(dba), **1**, and (bc)Pd(ns^X), $\mathbf{2^X}$, which have been the focus of our experimental investigations.[30,31] Ground-state-optimized structures of the model complexes (en)Pd(η^2-C_2H_4), **4**, and (en)Pd(η^2-O_2), **5**, are in excellent agreement with the corresponding experimental complexes. For example, the C−C bond length of the coordinated alkenes is 1.427(14) Å ($\mathbf{2^H}$) and 1.42 Å (**4**), and the O−O bond length of the activated O_2 (peroxo) moieties is 1.415(15) Å (**3**) and 1.42 Å (**5**). A metrical comparison of **4** and **5** is shown in Figure 2.

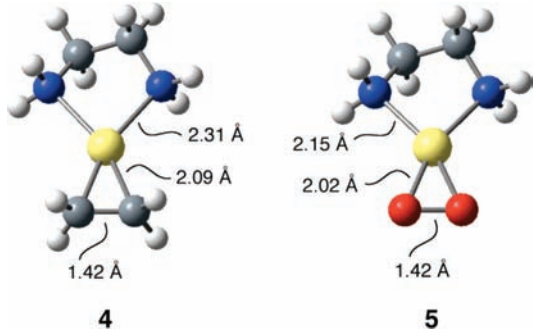

Figure 2. Ball-and-stick structures and metrics of the calculated ground-state complexes (en)Pd(C_2H_4), **4**, and (en)Pd(η^2-O_2), **5**.

The intermediate length of the C−C bond, relative to free ethylene (1.34 Å) and free ethane (1.54 Å),[32] in these and related late-transition-metal complexes reflects substantial back-bonding from the zerovalent Pd^0 center into the unfilled π^* orbital of the alkene.[33,34] Thus, the observed structure of **4**, as well as other Pd^0-alkene complexes, is best described as intermediate between the trigonal Pd^0-ethylene and square-planar Pd^{II}−metallacyclopropane resonance structures (eq 11).[35] Consistent with this description, natural charge (NC) analysis reveals substantial charge transfer from the (en)Pd fragment to ethylene: NC = −0.32 for ethylene, +0.32 for (en)Pd.

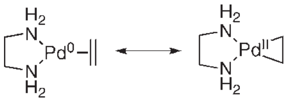

(11)

The structure of complex **5** features a lengthened O−O bond (1.42 Å), which is intermediate between the bond

---

(26) (a) Yamaguchi, K.; Jensen, F.; Dorigo, A.; Houk, K. N. *Chem. Phys. Lett.* **1988**, *149*, 537–542. (b) Yamanaka, S.; Kawakami, T.; Nagao, H.; Yamaguchi, K. *Chem. Phys. Lett.* **1994**, *231*, 25–33.

(27) The DFT-derived first excited-state energy of singlet dioxygen from the spin-contaminated singlet wave function is 10.3 kcal/mol, and is in considerable error based on the experimental energy (22.4 kcal/mol). The spin-projection correction improves the DFT-derived triplet-singlet energy difference to 20.6 kcal/mol.

(28) Harvey, J. N.; Aschi, M.; Schwarz, H.; Koch, W. *Theor. Chem. Acc.* **1998**, *99*, 95–99.

(29) See Figure S3 and the corresponding discussion in the Supporting Information.

(30) A previous study used ethylenediamine to model phenanthroline-derived ligands, see: Adams, D. M.; Noodleman, L.; Hendrickson, D. N. *Inorg. Chem.* **1997**, *36*, 3966–3984.

(31) See the Supporting Information for calculations supporting our use of ethylenediamine (en) to model the bathocuproine ligand in this study.

(32) *CRC Handbook of Chemistry and Physics*, 87th ed.; Lide, D. R., Ed.; CRC Press: Boca Raton, FL, 2006.

(33) (a) Dewar, M. J. S. *Bull. Soc. Chim. Fr.* **1951**, *18*, C71–C79. (b) Chatt, J.; Duncanson, L. A. *J. Chem. Soc.* **1953**, 2939–2947.

(34) The bonding in d^{10} Pd-alkene complexes has been the subject of numerous studies. For examples, see: (a) Ziegler, T.; Rauk, A. *Inorg. Chem.* **1979**, *18*, 1558–1565. (b) Kitaura, K.; Sakaki, S.; Morokuma, K. *Inorg. Chem.* **1981**, *20*, 2292–2297. (c) Ziegler, T. *Inorg. Chem.* **1985**, *24*, 1547–1552. (d) Morokuma, K.; Borden, W. T. *J. Am. Chem. Soc.* **1991**, *113*, 1912–1914. (e) Li, J.; Schreckenbach, G.; Ziegler, T. *Inorg. Chem.* **1995**, *34*, 3245–3252. (f) Uddin, J.; Dapprich, S.; Frenking, G.; Yates, B. F. *Organometallics* **1999**, *18*, 457–465.

(35) Commonly these complexes are characterized as Pd^0 species, except in cases in which strongly electron-deficient alkenes (e.g. tetracyanoethylene) are employed. Elsevier, Spek, and coworkers, however, have suggested that the Pd^{II} formal oxidation state may have greater general importance in the bonding description. van Asselt, R.; Elsevier, C. J.; Smeets, W. J. J.; Spek, A. L. *Inorg. Chem.* **1994**, *33*, 1521–1531.

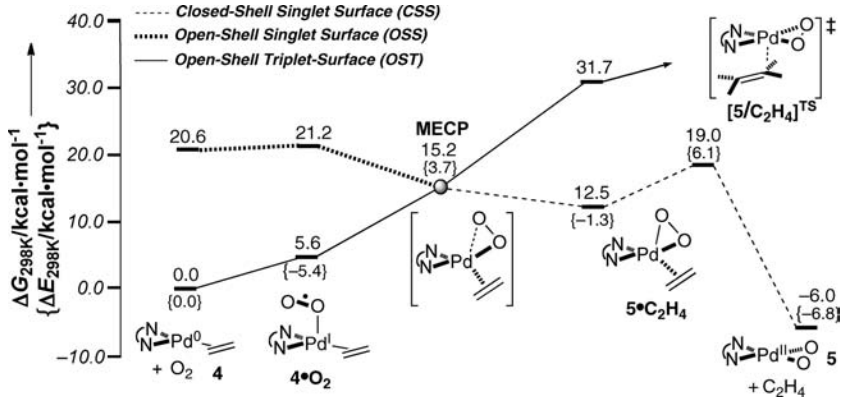

Figure 3. DFT-derived mechanism for associative oxygenation of (en)Pd(η^2-C_2H_4), **4**. The total energy in CH_2Cl_2 is presented in brackets {ΔE_{sol}}.

lengths of superoxide anion (1.33 Å) and peroxide dianion (1.49 Å).[36] Unlike the resonance formulation of Pd-alkene complexes, complex **5** is best described as a peroxo-Pd^{II} species possessing two covalent Pd−O bonds.[37] This description is supported further by a substantial increase of positive charge, NC = +1.04, on the (en)Pd fragment in **5**, relative to that in **4** (NC = +0.32).

Thermodynamics of Oxygenation of Palladium-Ethylene Derivatives. The free energy of oxygenation of **4** is calculated to be −6.4 kcal/mol (eq 12). This relatively low driving force for the reaction is in accord with our previous experimental observations that electron-deficient alkenes, such as the ns^X derivatives in eq 2, are capable of displacing O_2 from the Pd center (k_{rev}, eq 2).[9]

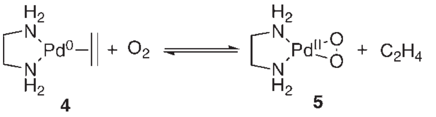

(12)

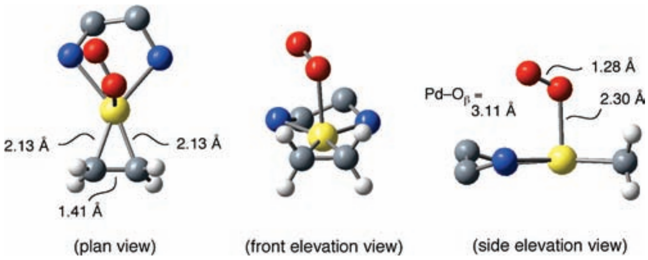

Figure 4. Ball-and-stick models of triplet η^1-superoxo-Pd^I intermediate **4·O₂**. Hydrogen atoms have been removed from the en ligand for clarity.

Mechanism of Ethylene/Dioxygen Substitution at Palladium: Overview. The oxygenation of **4** is initiated by an end-on approach of dioxygen at an axial-coordination site on the proximal face of the Pd center (Figure 3). The reaction occurs by single-electron transfer from Pd to O_2, yielding an η^1-superoxo-Pd^I intermediate (**4·O_2**). The formation of **4·O_2** is energetically favored by 5.4 kcal/mol on the open-shell-triplet (OST) total-energy surface; however, the intermediate is calculated to be uphill on the free-energy surface, owing to the entropic cost of the reaction. The open-shell-singlet (OSS) electronic state at the OST-optimized geometry is calculated to be 15.6 kcal/mol higher in energy than the OST electronic state (cf., 20.6 kcal/mol for dioxygen's calculated singlet, $^1\Delta_g$, excited-state energy). The OST surface increases in energy after intermediate **4·O_2**, as the distal oxygen atom is brought into proximity to the Pd center. This motion also causes the triplet and singlet spin-surfaces to merge at the MECP, where the energies of the two spin states are identical for the same geometry. Upon undergoing intersystem crossing at the MECP the axial superoxide ligand of **4·O_2** shifts toward an equatorial coordination site, vacating an axial coordination site of Pd to enable interaction with the distal oxygen of the η^1-superoxide ligand. (Note: Here and elsewhere, "equatorial" ligands are defined as those in the plane of the N−Pd−N atoms.) The geometric rearrangement about the Pd-coordination sphere facilitates the second single-electron transfer from Pd to O_2 and results in formation of an η^2-peroxo-Pd intermediate (**5·C_2H_4**) that is nearly 20 kcal/mol more stable on the CSS surface relative to the OST surface. Intermediate **5·C_2H_4** is stabilized slightly relative to the initial reactants on the total-energy surface (−1.3 kcal/mol), but it remains uphill on the free-energy surface (ΔG° = 12.5 kcal/mol). In the final step of the associative substitution reaction, the ethylene molecule dissociates from the Pd center via transition state **[5/C_2H_4]^{TS}** to yield complex **5** and free ethylene. The free energy of activation ($\Delta G^\ddagger$) arising from **[5/C_2H_4]^{TS}** is 19.0 kcal/mol. This value is higher than the MECP, suggesting that ethylene dissociation is the rate-limiting barrier for the overall transformation. The calculated free energy of activation, based on **[5/C_2H_4]^{TS}**, is reasonably close to the experimental value ($\Delta G^\ddagger$ = 21.4 kcal/mol) obtained from the temperature dependence of the rate of oxygenation of (bc)Pd(η^2-dba), **1**.[3a,d] In the following sections, we present a more-thorough analysis of the species identified in Figure 3.

Intermediate 4·O_2. Molecular oxygen reacts with complex **4** to yield intermediate **4·O_2**, which features a dioxygen ligand bound end-on at the axial face of the trigonal plane of complex **4** (Figure 4). The O−O bond is elongated (1.28 Å) in **4·O_2** relative to free dioxygen (1.21 Å), but is not as long as that observed in the one-electron-reduced, protonated superoxide radical (1.30 Å).[38] The side-on-coordinated ethylene molecule is essentially unaltered, with a very slightly shortened C−C bond length (0.01 Å) relative to **4**. This adduct is geometrically similar to an isoelectronic,

---

(36) Cotton, F. A.; Wilkinson, G.; Murillo, C. A.; Bochmann, M. *Advanced Inorganic Chemistry*; 6th ed.; Wiley: New York, 1999; p 450.

(37) For a more thorough discussion of bonding in late-transition-metal peroxide complexes, see: Cramer, C. J.; Tolman, W. B.; Theopold, K. H.; Rheingold, A. L. *Proc. Natl. Acad. Sci. U.S.A.* **2003**, *100*, 3635–3640.

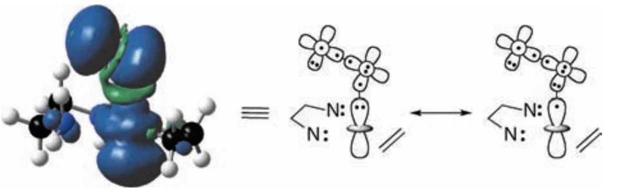

Figure 5. Natural-spin-density plot (darker/blue shade = alpha and lighter/green shade = beta spin orientation) and the corresponding localized Lewis-like resonance structures for the OST η^1-superoxo-Pd^{I} intermediate $\mathbf{4 \cdot O_2}$.

trigonal pyramidal Cu^{II}(η^1-superoxide) intermediate calculated by Cramer and Tolman along the pathway for the associative oxygenation of a (β-diketiminate)Cu^{I}(THF) complex.[10c,39]

The lowest energy state of $\mathbf{4 \cdot O_2}$ has a triplet electronic configuration, which mirrors the ground-state electronic configuration of free dioxygen. However, the intermediate length of the O$-$O bond in $\mathbf{4 \cdot O_2}$ suggests that the dioxygen moiety has been reduced via charge transfer from the Pd center. Analysis of the natural spin-density (NSD) of the OST configuration reveals that the unpaired spin is delocalized over the dioxygen moiety ($O_\alpha = 0.79$ and $O_\beta = 0.69$) and Pd center (0.48). Visualization of the NSD suggests that one of the two unpaired electrons is accommodated by a 2-center, 3-electron bonding interaction between a Pd-based d-orbital with approximately d_{z^2} character and the $\pi_{\parallel}$* orbital of O_2 (Figure 5). The second unpaired electron remains localized in the other $\pi_{\perp}$* orbital of O_2, which maintains exchange stabilization and the observed lower energy OST state.

The electronic structure of OST intermediate $\mathbf{4 \cdot O_2}$ is described as a resonance between a Pd^0-dioxygen and biradical-Pd^{I}(η^1-O_2) species (Figure 5). The latter electronic configuration reflects the observed lengthening of the O$-$O bond in $\mathbf{4 \cdot O_2}$ as well as the unpaired spin-density residing on the Pd center, and thus represents the major resonance contribution. Natural-charge (NC) analysis indicates substantial positive charge build-up in the (en)Pd fragment of $\mathbf{4 \cdot O_2}$ relative to complex **4** (+0.75 and +0.32, respectively). The ethylene ligand is also found to retain a significant negative charge upon coordination of O_2 (NC = -0.32 and -0.27 in complexes **4** and $\mathbf{4 \cdot O_2}$, respectively). These observations support the formal oxidation state assignment for Pd as +1.

Minimum-Energy Crossing Point. As expected, the coordination geometry of the MECP (Figure 6) is intermediate between OST intermediate $\mathbf{4 \cdot O_2}$ and CSS intermediate $\mathbf{5 \cdot C_2H_4}$. Specifically, the length of the O$-$O bond (1.33 Å) reflects the one-electron reduced superoxide character of the dioxygen moiety; whereas, the length of the Pd$-$O$_\beta$ interaction (2.47 Å) and the slippage of the ethylene molecule to an axial/equatorial coordination geometry is approaching the pseudo-octahedral geometry evident in $\mathbf{5 \cdot C_2H_4}$ (vide infra). This ligand reorganization leads to improved orbital overlap between a singly occupied molecular orbital localized on Pd and the singly occupied $\pi_{\perp}$* orbital on the O_2 moiety.

Intermediate $\mathbf{5 \cdot C_2H_4}$ and Transition State $\mathbf{[5/C_2H_4]^{TS}}$. After accessing the MECP, the CSS and OST surfaces diverge in energy. The CSS surface becomes more stable and leads to the formation of metastable intermediate $\mathbf{5 \cdot C_2H_4}$ ligated by both ethylene and dioxygen molecules (Figure 7). The geometry of the intermediate features a six-coordinate ligand environment in which the equatorial Pd$-$O and Pd$-$C bond lengths (1.99 Å and 2.15 Å, respectively) are shorter than the corresponding axial Pd$-$O and Pd$-$C bond lengths (2.18 Å and 2.19 Å, respectively). This geometric arrangement resembles an octahedral ligand field. The O$-$O and C$-$C bonds (both 1.39 Å) are lengthened relative to free dioxygen (1.21 Å) and ethylene (1.34 Å) reflecting the reduced nature of both molecules. The resonance limit of this bonding description corresponds to a Pd^{IV}-type electronic configuration (i.e., (η^2-peroxo)Pd^{IV}-metallacyclopropane) (eq 13).

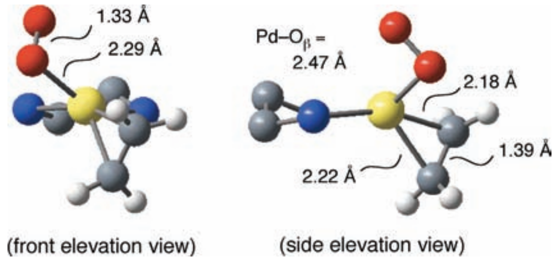

Figure 6. Ball-and-stick models of the MECP. Hydrogen atoms have been removed from the en ligand for clarity.

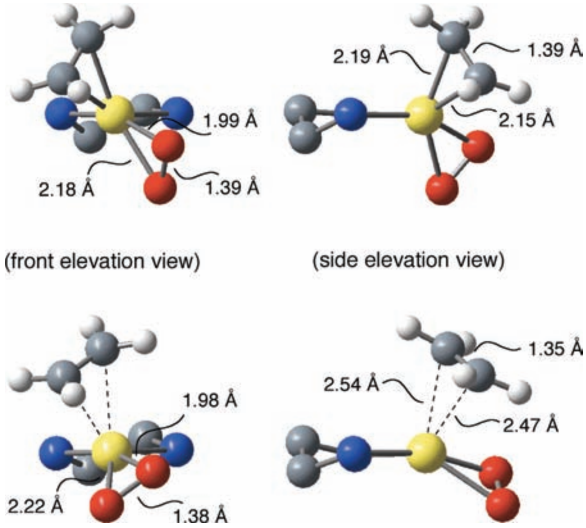

Figure 7. Ball-and-stick models of CSS intermediate $\mathbf{5 \cdot C_2H_4}$ (top structures) and transition-state $\mathbf{[5/C_2H_4]^{TS}}$ (bottom structures). Hydrogen atoms have been removed from the en ligand for clarity.

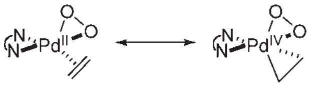

(13)

Formation of product **5** occurs via dissociation of ethylene from the axial face of the Pd-complex via transition-state $\mathbf{[5/C_2H_4]^{TS}}$. The Pd$-$C bond lengths are similar (2.47 and 2.54 Å), and the shortened C$-$C bond length (1.35 Å) reflects oxidation of the ethylene fragment relative to intermediate $\mathbf{5 \cdot C_2H_4}$ (Figure 7). To better understand the electronic effects along the CSS surface connecting intermediate $\mathbf{5 \cdot C_2H_4}$ and Pd^{II}(η^2-O_2) **5**, we

---

[38] Smith, D. W.; Andrews, L. *J. Chem. Phys.* **1974**, *60*, 81–85.

[39] Heppner, D. E.; Gherman, B. F.; Tolman, W. B.; Cramer, C. J. *Dalton Trans.* **2006**, 4773–4782.

Table 1. NBO-Derived Natural Charges for the (en)Pd Fragment, Ethylene, And Dioxygen along the Calculated Closed-Shell Singlet Total Energy Surface for Ethylene Association/Dissociation at Complex **5**[a]

	$\mathbf{5 \cdot C_2H_4}$	$\mathbf{[5/C_2H_4]^{TS}}$	$\mathbf{5C/C_2H_4}$	$\mathbf{5{+}C_2H_4}$
(en)Pd	+1.04	+1.01	+0.97	+0.93
C_2H_4	−0.11	−0.08	−0.01	0.00
O_2	−0.93	−0.93	−0.96	−0.93

[a] See Supporting Information, Figure S2.

Figure 8. NBOView plots illustrating the principal orbital interactions along the closed-shell-singlet total energy surface. **5C/C$_2$H$_4$** ($d_{\text{Pd-C(proximal)}}$ = 3.5 Å), see Supporting Information, Figure S2.

Figure 9. NBOView plot illustrating the principal orbital interaction involved in the degenerate ethylene exchange transition state at (di)Pd(η^2-C$_2$H$_4$) (di = ethylenediimine).[7b]

examined geometries along the intrinsic reaction coordinate defined by transition state $\mathbf{[5/C_2H_4]^{TS}}$ (Supporting Information, Figure S2). Over the CSS surface, electron density is transferred from the ethylene ligand to the Pd center, as determined by natural charge analysis (Table 1). The reverse is true for displacement of dioxygen from complex **5** (cf. k_{rev}, eq 2). Namely, a d$_{z^2}$-like Pd orbital attacks the π^* orbital of ethylene as depicted by the principal natural-bond-orbital interaction in **5C/C$_2$H$_4$**, a structure obtained from the intrinsic reaction coordinate connecting $\mathbf{[5/C_2H_4]^{TS}}$ to **5** and C$_2$H$_4$ (Figure 8).

Similarity between Associative Oxygenation and Alkene−Alkene Exchange at Pd(η^2-alkene) Complexes. We have previously reported experimental and computational studies of the mechanism of alkene substitution reactions involving the Pd(η^2-alkene) complexes $\mathbf{2^X}$ (see Introduction, eq 3).[7] The electronic effects on the rate of these alkene substitution reactions contradicted the classical mechanism for associative ligand substitution reactions, which involves interaction of the highest occupied molecular orbital (HOMO) of the incoming ligand (alkene, in this case) with the metal-based lowest unoccupied molecular orbital (LUMO). Rather, the studies revealed that electron-rich Pd^0 species $\mathbf{2^X}$ interacts most strongly with the incoming ligand via donation of electron density from Pd into the π^* orbital of the incoming alkene (Figure 9). These insights underlie the description of these reactions as "inverse-electron-demand" ligand substitution reactions.

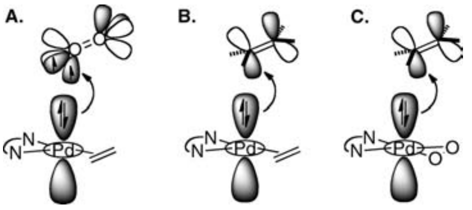

Figure 10. Comparative illustration of the similar frontier-orbital donor−acceptor interactions in (A) oxygenation at Pd^0(η^2-alkene), (B) associative alkene substitution at Pd^0(η^2-alkene) and (C) "oxidatively-induced" reductive elimination of dioxygen from Pd$^{\text{II}}$(η^2-O$_2$).[40]

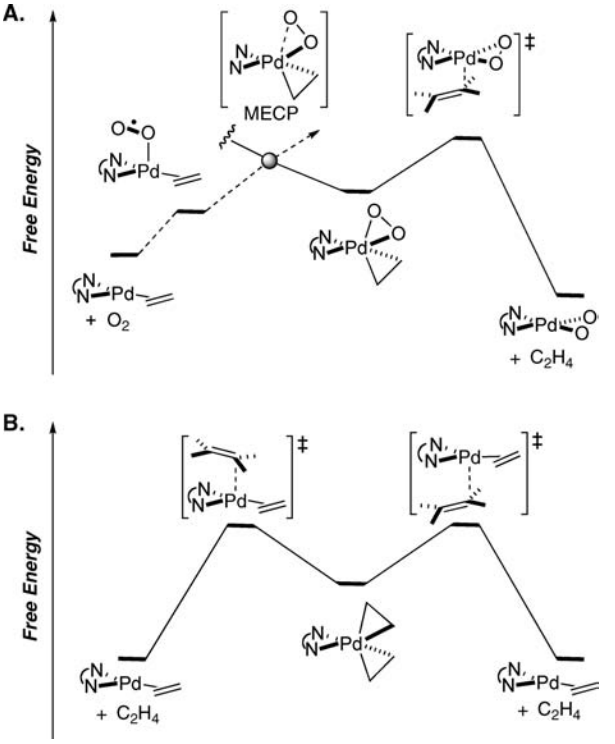

Figure 11. Qualitative depiction of the associative reaction coordinates for (A) oxygenation and (B) degenerate exchange of ethylene at Pd^0(η^2-C$_2$H$_4$). The dashed and solid lines refer to the triplet and singlet free energy surfaces, respectively.

Although dioxygen and alkenes have different spin states and redox potentials, the orbital interactions that guide exchange reactions at Pd(η^2-alkene) and Pd(η^2-O$_2$) complexes present similar profiles. For exchange of Pd(η^2-alkene) with another alkene or O$_2$, the initial interaction involves charge transfer from a Pd-based lone pair into the π^* orbital of the substrate (Figures 10A and 10B). Displacement of O$_2$ from Pd$^{\text{II}}$(η^2-O$_2$) species by electron-deficient alkenes (Figure 10C, cf. eq 2, k_{rev}) exhibits similar donor (Pd lone pair) to acceptor (alkene π^*) orbital interactions.[40] These similarities overshadow differences in fact, such as the open-shell triplet character of O$_2$ with a singly occupied π^* acceptor versus the closed-shell alkene with an empty π^* acceptor orbital, and in formalism, such as the change in Pd oxidation state for reactions that lose or gain O$_2$ versus the retention of Pd^0 oxidation state for alkene−alkene exchange reactions.

The similarity between dioxygen and alkenes is further emphasized by inspection of the overall mechanisms of their reactions with (en)$Pd^0(C_2H_4)$ (Figure 11). Both pathways proceed through singlet pseudo-octahedral intermediates. The resemblance to more-traditional octahedral metal centers draws attention to the π-acidic nature of both O_2 and alkenes in their interaction with the Pd center. The main difference in the pathways arises from the differing electronic structures for triplet dioxygen and singlet alkene. For dioxygen, single-electron-transfer from Pd to a singly occupied π^* orbital is enthalpically favored, and thus yields a $Pd^I(\eta^1$-superoxide) intermediate (**$4\cdot O_2$**). An analogous η^1 intermediate is not formed in the reaction of the alkene; rather, species resembling the η^1 intermediate are formed as a transition state leading to formation of the pseudo-octahedral intermediate. In fact, this transition state closely resembles the MECP structure on the O_2 reaction pathway, which connects the η^1-superoxide adduct to the pseudo-octahedral (en)Pd(η^2-O_2)(η^2-alkene) intermediate.

Conclusion

This DFT study builds upon our previous experimental and computational studies and illustrates important mechanistic features of the reaction of O_2 with Pd^0-alkene complexes. The work reinforces our prior suggestion that simple alkenes and molecular oxygen react at Pd via similar pathways,[3d,9] and the studies provide a useful model for understanding the nature of interaction between Pd and molecular oxygen.[41] The formation of a $Pd^I(\eta^1$-superoxide) intermediate, which was identified previously from computational analysis of the reaction of O_2 with a simple (en)Pd^0 fragment, is also evident in the reaction of O_2 with the experimentally more-relevant (en)Pd(η^2-C_2H_4) complex. This intermediate appears to facilitate the reaction of triplet O_2 with a closed-shell transition-metal center by delocalizing spin density onto the metal center, thereby reducing the energy gap between the triplet and singlet spin surfaces. Extension of this study toward the direct examination of the reactivity of dioxygen and benzoquinone at Pd^0 species bearing catalytically relevant ancillary ligands is presently underway.

Acknowledgment. We thank the following organizations for financial support and access to computational resources: NSF (CHE-0543585), TeraGrid (CHE-070040N), UW Parallel Computing Center (CHE-0091916), and gifts from Intel Corporation.

Supporting Information Available: Benchmarking results, tabulated data, structural coordinates, complete citations for Gaussian 98 and Gaussian 03. This material is available free of charge via the Internet at http://pubs.acs.org.

---

(40) The displacement of O_2 from Pd(η^2-O_2) with alkene can be described as an oxidatively induced reductive elimination reaction. Such reactions have a rich history in late-transition-metal organometallic chemistry, see for example:(a) Kochi, J. K. *Organometallic Mechanisms and Catalysis*; Academic Press: New York, 1978. (b) Yamamoto, T.; Yamamoto, A.; Ikeda, S. *J. Am. Chem. Soc.* **1971**, *93*, 3350–3359. (c) Tsou, T. T.; Kochi, J. K. *J. Am. Chem. Soc.* **1979**, *101*, 7547–7560. (d) Tatsumi, K.; Nakamura, A.; Komiya, S.; Yamamoto, A.; Yamamoto, T. *J. Am. Chem. Soc.* **1984**, *106*, 8181–8188. (e) Komiya, S.; Akai, Y.; Tanaka, K.; Yamamoto, T.; Yamamoto, A. *Organometallics* **1985**, *4*, 1130–1136.

(41) The description of open-shell $Pd^I(\eta^1$-superoxide)(η^2-alkene) presented here may also prove to be relevant in the aerobic oxidation of organometallic Ir^I- and $Rh^I(\eta^2$-alkene) complexes. For recent reviews highlighting this chemistry, see: (a) Hetterscheid, D. G. H.; de Bruin, B. *J. Mol. Catal. A: Chem.* **2006**, *251*, 291–296. (b) Tejel, C.; Ciriano, M. A. *Top. Organomet. Chem.* **2007**, *22*, 97–124.